Research Square

Preprints are preliminary reports that have not undergone peer review.
They should not be considered conclusive, used to inform clinical practice,
or referenced by the media as validated information.

A Closed-Form Analytic Formulation of the PMNS Lepton Mixing Matrix

Pramod Kumar Meher

pkmeher@cgu-odisha.ac.in

* C. V. Raman Global University https://orcid.org/0000-0003-0992-1159

Research Article

Keywords: PMNS Matrix, Flavour Physics, Neutrino mixing

Posted Date: October 8th, 2026

DOI: https://doi.org/10.21203/rs.3.rs-10958595/v2

License: This work is licensed under a Creative Commons Attribution 4.0 International License.
Read Full License

Additional Declarations: The authors declare no competing interests.

A Closed-Form Analytic Formulation of the PMNS Lepton Mixing Matrix

Pramod Kumar Meher

C. V. Raman Global University,
Bhubaneswar, Odisha, India, 752054;
pkmeher@gmail.com

Abstract

We extend the quark-sector *mixing-equilibrium condition* to the lepton sector, postulating:

$$\alpha_\ell(1-\alpha_\ell) = \mathcal{C}_\ell \lambda^2,$$

where α_ℓ is the *equilibrium mixing-weight*, $(1-\alpha_\ell)$ the *equilibrium retention-weight*, and $\mathcal{C}_\ell = 1 + (B-L)/2$ the coupling factor with lepton gauge charge $(B-L) = -1$, using the universal *fermion mixing constant* $\lambda = 1/(\pi\sqrt{2})$. We show that quarks and leptons are dual electroweak configurations whose mixing patterns are determined by the $(B-L)$ quantum number.

Based on this condition, we deduce a closed-form analytic formulation of the mixing angles, Dirac CP phases, and the leptonic Jarlskog invariant, determining the Pontecorvo–Maki–Nakagawa–Sakata (PMNS) lepton mixing matrix. We find the solar angle $\sin^2\theta_{12} = \frac{1}{3} - \frac{\lambda^2}{2} \approx 0.3080$ $(+0.08\sigma)$, reactor angle $\sin^2\theta_{13} = \frac{\lambda^2}{2} - \frac{\lambda^3}{3} \approx 0.0215$ (-0.89σ), and upper-octant atmospheric angle $\sin^2\theta_{23} = \frac{1}{2} + \lambda^2 \approx 0.5507$ $(\theta_{23} \approx 47.91^\circ, -0.51\sigma)$. The Dirac CP phases and Jarlskog invariants are obtained as $\delta_{\mathrm{CP,NO}} \approx 181.49^\circ$ ($J_{\mathrm{CP}}^{\mathrm{NO}} \approx -0.000858$, 0.75σ pull) and $\delta_{\mathrm{CP,IO}} \approx 283.1^\circ$ ($J_{\mathrm{CP}}^{\mathrm{IO}} \approx -0.0321$, 0.26σ pull), mapping directly from the two-state equilibrium structure.

The lepton fermion mixing constant $\alpha_\ell \approx 0.026000$, derived from the condition $\alpha_\ell(1-\alpha_\ell) = \mathcal{C}_\ell\lambda^2 = 1/(4\pi^2)$, is ≈ 2.3 times smaller than the quark fermion mixing constant $\alpha_q \approx 0.063084$, rendering the lepton sector relatively more compliant (less rigid) in its mixing structures compared to the quark sector, allowing it to generate large mixing angles

The same constant λ underpins the closed-form formulation of the CKM quark mixing matrix without free parameters, demonstrating that a single universal invariant prevails in both quark and lepton flavour mixing.

1 Introduction

The discovery of neutrino oscillations across solar, atmospheric, reactor, and accelerator experiments has established that neutrinos possess non-zero masses and mix significantly across generations [1, 2, 3, 4, 5, 6]. In the Standard Model, flavour mixing in the leptonic sector is described by the Pontecorvo–Maki–Nakagawa–Sakata (PMNS) matrix [7, 1, 8], in direct analogy to quark flavour mixing parameterized by the unitary Cabibbo–Kobayashi–Maskawa (CKM) matrix [8]. The PMNS matrix relates the neutrino flavour eigenstates $(\nu_e, \nu_\mu, \nu_\tau)$ to the mass eigenstates (ν_1, ν_2, ν_3) in the standard Particle Data Group (PDG) parameterization, where $s_{ij} \equiv \sin\theta_{ij}$ and $c_{ij} \equiv \cos\theta_{ij}$:

$$U_{\mathrm{PMNS}} = \begin{pmatrix} c_{12}c_{13} & s_{12}c_{13} & s_{13}e^{-i\delta_{\mathrm{CP}}} \\ -s_{12}c_{23} - c_{12}s_{23}s_{13}e^{i\delta_{\mathrm{CP}}} & c_{12}c_{23} - s_{12}s_{23}s_{13}e^{i\delta_{\mathrm{CP}}} & s_{23}c_{13} \\ s_{12}s_{23} - c_{12}c_{23}s_{13}e^{i\delta_{\mathrm{CP}}} & -c_{12}s_{23} - s_{12}c_{23}s_{13}e^{i\delta_{\mathrm{CP}}} & c_{23}c_{13} \end{pmatrix}, \tag{1}$$

serving as the fundamental unitary bridge mapping the weak-interaction eigenbasis to the free-propagation mass eigenbasis. Beyond the standard PDG convention, historical and ongoing efforts to characterize it have explored diverse parameterization schemes, including Wolfenstein-like expansions around tri-bimaximal mixing baselines in powers of $|U_{e3}|$ and exponential representations that explicitly separate CP-violating and Majorana phases from rotational blocks [9, 10].

To move beyond purely phenomenological parametrizations, various analytical and model-dependent derivations have been proposed in the literature. These range from gauge-Higgs unification models in warped extra dimensions [11] and discrete non-Abelian flavour symmetries [12, 13, 14, 15] to heuristic "parameter-free" attempts utilizing microscopic spin interactions [16] or scalar wavefunction geometries [17, 18]. However, these alternative analytic attempts suffer from fundamental shortcomings: they either rely on unphysical mechanical toy models with hidden adjustable parameters, or they fail to achieve rigorous, sub-1σ agreement with modern high-precision global oscillation data (such as NuFIT 6.0 and PDG 2024). A closed-form analytic model that reproduces the mixing parameters and associated quantities could provide useful insight into the neutrino mixing mechanism. Yet, a predictive framework of this type has not yet been established.

While the Standard Model accommodates flavour mixing patterns through empirical inputs, it provides no clear rationale for their observed structures. The core of the flavour puzzle lies in the stark, unexplained contrast between hierarchically small quark mixing angles and large lepton mixing angles. Table 1 places the key distinctions side by side, highlighting that quark mixing is hierarchically small across all three angles and CP violation is heavily suppressed, whereas lepton mixing is large in two of the three angles and the leptonic Jarlskog invariant $J^{\ell}_{\rm CP}$ is nearly three orders of magnitude larger than its quark counterpart. In this work, we establish that this contrast arises from the sign of the $(B-L)$ gauge charge rather than from fine-tuned Yukawa hierarchies. Although proposals like Quark–Lepton Complementarity ($\theta^q_{12}+\theta^{\ell}_{12}\approx 45^\circ$) have attempted to link the two sectors [19, 20], they typically rely on ad hoc symmetry assumptions or post-hoc parameter fits without explaining why the underlying electroweak vacuum structure enforces a rigid coupling for quarks and a compliant configuration for leptons.

Table 1: Contrasting features of quark and lepton mixing based on PDG 2024 and NuFIT data.

Phenomenological Property	Quark Sector (CKM)	Lepton Sector (PMNS)
Primary mixing angle (θ_{12})	$\theta^q_{12}\approx 13.0^\circ$ (Small)	$\theta^{\ell}_{12}\approx 33.4^\circ$ (Large)
Second-generation mixing (θ_{23})	$\theta^q_{23}\approx 2.4^\circ$ (Hierarchical)	$\theta^{\ell}_{23}\approx 49.0^\circ$ (Near-maximal)
Cross-generation mixing (θ_{13})	$\theta^q_{13}\approx 0.2^\circ$ (Suppressed)	$\theta^{\ell}_{13}\approx 8.5^\circ$ (Moderately large)
Dirac CP-violating phase ($\delta_{\rm CP}$)	$\delta^{\rm CKM}_{\rm CP}\approx 65.5^\circ$	$\delta^{\rm PMNS}_{\rm CP}\sim 197^\circ$–$230^\circ$ (NO) / 274°–285° (IO)
Jarlskog CP invariant ($J_{\rm CP}$)	$J^q_{\rm CP}\approx +3.0\times 10^{-5}$	$\lvert J^{\ell}_{\rm CP}\rvert \lesssim 0.033$ (Order 10^{-2})

In this work, we extend the closed-form analytical formulation recently developed for quark flavour mixing [21] to the leptonic sector. In that companion work, the *fermion mixing constant* is defined as $\lambda = 1/(\pi\sqrt{2})$ in direct relation to the Cabibbo angle, establishing that $(1-\alpha_q)=\sin\delta_{13}$ through the fundamental mixing equilibrium condition $\alpha_q(1-\alpha_q)=\mathcal{C}_q\lambda^2=7/(12\pi^2)$, where $\mathcal{C}_q$ denotes the *coupling factor of the quark sector*. The *equilibrium mixing-weight* $\alpha_q\approx 0.063084$ is identified with the Weinberg-angle ratio $\tan^2(\theta_W/2)=(M_Z-M_W)/(M_Z+M_W)\approx 0.063012$ as the quark-sector electroweak invariant. The lepton sector carries its own *equilibrium mixing-weight* $\alpha_\ell\approx 0.026000$ (with complement $1-\alpha_\ell\approx 0.974000$), defined through the *lepton mixing equilibrium condition* $\alpha_\ell(1-\alpha_\ell)=\mathcal{C}_\ell\lambda^2=1/(4\pi^2)$. Both equilibria share the same fermion mixing constant λ;

only the coupling factors $\mathcal{C}_q$ and $\mathcal{C}_\ell$ of the quark and lepton sectors distinguish them. Building upon the quark sector results, the present paper demonstrates that using the same underlying condition, the leptonic sector naturally generates large PMNS mixing angles and near-maximal CP violation.

The remainder of the paper is organised as follows. Section 2 reviews the fundamentals, including the significance of the fermion mixing constant λ, and introduces the lepton sector equilibrium mixing-weight and the unified mixing equilibrium condition for both quark and lepton sectors. Section 3 formulates the three PMNS mixing angles in closed form. Besides, it derives the expression for the leptonic Dirac CP phase and evaluates the Jarlskog invariant $J^{\ell}_{\rm CP}$. Section 4 calculates the numerical values of the PMNS matrix and discusses quark–lepton duality. Section 5 summarises the results and outlines specific experimental tests at forthcoming neutrino facilities.

Table 2: Key symbols, descriptions, and their contexts of origin.

Symbol	Description	Defining Context
λ	Fermion fermion mixing constant	$1/\lambda^2 = 2\pi^2$ ($\mathrm{SU}(2)_L$ Haar volume)
D_q	$(B-L)$ quantum number of quarks	$D_q \equiv (B-L)_q : D_q = 1/3$
D_ℓ	$(B-L)$ quantum number of leptons	$D_\ell \equiv (B-L)_\ell : D_\ell = -1$
$\mathcal{C}_q$	Quark coupling factor	$\mathcal{C}_q = 1 + D_q/2 : \mathcal{C}_q = 7/6$
$\mathcal{C}_\ell$	Lepton coupling factor	$\mathcal{C}_\ell = 1 + D_\ell/2 : \mathcal{C}_\ell = 1/2$
α_i	Equilibrium mixing-weight	Equilibrium condition: $\alpha_i(1-\alpha_i) = \lambda^2\mathcal{C}_i$
$1-\alpha_i$	Equilibrium retention-weight	Equilibrium condition: $\alpha_i(1-\alpha_i) = \lambda^2\mathcal{C}_i$

$i = q$ refers to quark sector and $i = \ell$ refers to lepton sector.

2 Key Quark-Lepton Flavour Invariants

2.1 The GMN Charge Partition and Sector Coupling Factors

In the left–right symmetric model (LRSM) with gauge group $\mathrm{SU}(2)_L \otimes \mathrm{SU}(2)_R \otimes \mathrm{U}(1)_{B-L}$, the electric charge of a left-handed fermion is determined by the Gell-Mann–Nishijima (GMN) relation [22, 23]:

$$Q = T_3 + \frac{D}{2}, \tag{2}$$

where $D = B - L$ *gauge charge* and T_3 is the third component of weak isospin. Applying it to the left-handed lepton doublet $(B = 0, L = 1)$, we get:

$$\frac{D_\ell}{2} = \frac{0-1}{2} = -\frac{1}{2}, \tag{3}$$

which gives the doublet assignments listed in Table 3 and displayed on the $\mathrm{SU}(2)_L$ isospin circle in Fig. 1. For the left-handed quark doublet $(B = 1/3, L = 0)$, $(D_q/2) = +1/6$, giving $T_3(u_L) = +1/2$ and $T_3(d_L) = -1/2$ as usual. The contrast $(D_\ell/2) = -1/2$ versus $(D_q/2) = +1/6$ is the fundamental origin of the quark–lepton mixing asymmetry.

Since the $(B-L)$ gauge charge has a significant impact on the flavour mixing of each sector, we define the *sector coupling factor* as:

$$\mathcal{C} = 1 + \frac{B-L}{2}, \tag{4}$$

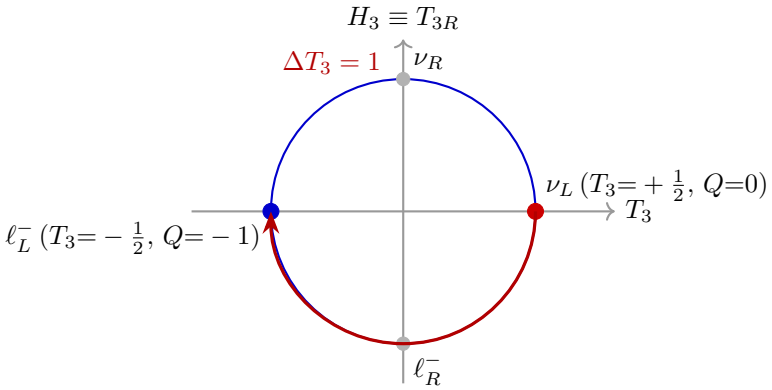


Figure 1: The $\mathrm{SU}(2)_L \otimes \mathrm{SU}(2)_R$ isospin manifold for leptons (invariant circle $T_3^2 + H_3^2 = 1/4$). Left-handed states lie on the T_3 axis; right-handed states on the $H_3 \equiv T_{3R}$ axis. The red arc shows the full isospin traversal $\Delta T_3 = 1$ between the charged-lepton and neutrino doublet members.

which measures the degree to which the sector's $(B - L)$ quantum number constrains the flavour transitions. Evaluated for the two sectors:

$$\mathcal{C}_q = 1 + \frac{1}{6} = \frac{7}{6} > 1 \quad \text{(quarks: stronger flavour coupling)}, \tag{5}$$

$$\mathcal{C}_\ell = 1 - \frac{1}{2} = \frac{1}{2} < 1 \quad \text{(leptons: weaker flavour coupling)}, \tag{6}$$

With $\mathcal{C}_q > 1$, the quarks offer relatively higher flavour mixing, resulting in smaller mixing angles (CKM). With $\mathcal{C}_\ell < 1$, leptons offer lower flavour mixing, resulting in large lepton mixing angles (PMNS). The mixing equilibrium conditions that determine the sector-specific parameters are defined in Section 2.2. Table 3 contains the electroweak quantum numbers of all three lepton generations. The critical entry is the last column: the coupling factor $\mathcal{C}_\ell = 1/2$ is identical across every row, reflecting the uniform $B - L = -1$ of all active leptonic doublets. It is this constant sub-unity coupling that results in the cross-generation mixing barrier and drives the large PMNS mixing angles derived in the following sections.

Table 3: Quantum numbers of three generations of the active leptonic $\mathrm{SU}(2)_L$ doublets.

Generation (i)	Lepton Component	Q	T_3	$D_\ell/2$	$B - L$	$\mathcal{C}_l = 1 + D_\ell/2$
$i = 1$	ν_{eL}	0	+1/2	−1/2	−1	1/2
	ℓ_L^-	−1	−1/2	−1/2	−1	1/2
$i = 2$	$\nu_{\mu L}$	0	+1/2	−1/2	−1	1/2
	μ_L^-	−1	−1/2	−1/2	−1	1/2
$i = 3$	$\nu_{\tau L}$	0	+1/2	−1/2	−1	1/2
	τ_L^-	−1	−1/2	−1/2	−1	1/2

2.2 Sector-Invariant Fermion Mixing Constant and Equilibrium Mixing-Weight

2.2.1 The Fermion Mixing Constant (λ).

It is defined as

$$\lambda = \frac{1}{\pi\sqrt{2}} \approx 0.225079. \tag{7}$$

It is sector-invariant, since the same λ appears in the mixing equilibrium condition for both quark and lepton mixing. Its physical significance is discussed in detail in the companion paper on the analytical construction of the CKM matrix [21]. The relevance of λ in flavour mixing is outlined here:

i. *Haar Measure.* $\lambda^2 = 1/(2\pi^2)$ equals the normalisation factor of the invariant Haar measure on $\mathrm{SU}(2)_L$, whose total group volume is $\mathrm{Vol}(\mathrm{SU}(2)_L) = 2\pi^2$ [24].

ii. *Phase Normalised Charge Transfer.* $\lambda = (1/\sqrt{2})(1/\pi)$ arises from the product of the symmetric inter-generation overlap factor $1/\sqrt{2}$ and the charge transfer $\Delta Q/\Delta\Phi = 1/\pi$ normalised over the full $\mathrm{SU}(2)_L$ phase interval $\Delta\Phi = \pi$ [21].

iii. *Cabibbo Correspondence.* The defined value of $\lambda = 0.225079$ coincides with $\sin\theta_C \approx 0.22500 \pm 0.00067$ (PDG global CKM fit) to within 0.04%, confirming its correspondence with high experimental precision. This directly relates to charge migration during flavour mixing.

iv. *Sector Universality.* λ remains the same for the quark and lepton sectors and impacts mixing in both sectors.

2.3 The Generalised Mixing Equilibrium Condition

The *mixing-equilibrium condition* for both quarks and lepton flavours is postulated as

$$\alpha_i(1-\alpha_i) = \mathcal{C}_i\,\lambda^2, \tag{8}$$

where $0 < \alpha_i < 1-\alpha_i$ represents the *equilibrium mixing-weight* of the respective sector ($i = q$ for quarks and $i = \ell$ for leptons), $(1-\alpha_i)$ is the corresponding *retention-weight*, and λ is the fermion mixing constant given by (7). As defined in (5) and (6), the coupling factor for the quark sector is $\mathcal{C}_q = 7/6$, and for the lepton sector, the coupling factor $\mathcal{C}_\ell = 1/2$. The quark sector equilibrium mixing-weight is determined as the smaller root of the quark-sector mixing equilibrium condition [21]:

$$\alpha_q(1-\alpha_q) = \mathcal{C}_q\,\lambda^2 = \frac{7}{12\pi^2}, \tag{9}$$

giving $\alpha_q \approx 0.063084$. The relevance of α_q in flavour mixing is outlined here:

i. *Electroweak Identification.* $\alpha_q = \tan^2(\theta_W/2) = (M_Z - M_W)/(M_Z + M_W) \approx 0.063012$, confirmed independently by precision electroweak measurements. α_q is thus a directly measurable electroweak invariant.

ii. *Role in Quark Mixing.* Together with λ, it generates the complete CKM matrix without any other parameter. It impacts flavour mixing of all higher generations of quark flavour mixing [21].

iii. *CP Phase Link.* The state retention-weight is obtained by larger root $(1-\alpha_q) \approx 0.937$ of (9) which satisfies $\sin\delta_{13} \approx 0.932 \pm 0.015$, linking the CKM Dirac CP-violating phase directly to the quark-sector mixing equilibrium condition.

iv. *Single-Parameter Determination.* Given λ, α_q is fully determined by $\mathcal{C}_q$ alone according to (9), which is fixed to 7/6 for all quark states; no further freedom exists once the gauge group and $(B-L)$ quantum numbers are specified.

2.4 The Lepton Sector Equilibrium Mixing Weight (α_l)

The *equilibrium mixing-weight* of the lepton sector is the smaller root of the lepton-sector *mixing equilibrium condition* constrained by λ and lepton coupling $\mathcal{C}_\ell$:

$$\alpha_l(1-\alpha_l) = \mathcal{C}_\ell\,\lambda^2 = \frac{1}{4\pi^2}, \tag{10}$$

giving $\alpha_l \approx 0.02599978$ for $\mathcal{C}_\ell = 1/2$ (with its complementary component $1-\alpha_l \approx 0.97400022$). The same λ governs both equilibria; only the coupling factor changes with sector. It is in direct analogy with α_q defined for the quark sector by the similar relation (9). Its principal properties are:

i. *CP Phase Correspondence.* It is interesting to note that $\arcsin(1-\alpha_l) \approx 76.90^\circ$ enters the PMNS Dirac CP phase as the lepton-sector higher-generation mixing shift, encoding the role that α_l plays in the PMNS mixing angles as the lepton-sector analogue of α_q in the quark sector.

ii. *Equilibrium Variance and CP-Phase Product.* The quantity $\alpha_l(1-\alpha_l)$ is the *lepton equilibrium variance*. The two roots α_l (smaller) and $1-\alpha_l$ (larger) are the sine projections of the dual CP-violating phases: $\alpha_l = \sin(\delta_{\mathrm{CP,NO}} - 180^\circ)$ and $1-\alpha_l = \sin(\delta_{\mathrm{CP,IO}} - 180^\circ)$. The mixing equilibrium condition (10) is therefore equivalently a constraint on the *product* of these sine projections:

$$\sin(\delta_{\mathrm{CP,NO}} - 180^\circ)\cdot\sin(\delta_{\mathrm{CP,IO}} - 180^\circ) = \mathcal{C}_\ell\,\lambda^2 = \tfrac{1}{4\pi^2}, \tag{11}$$

verified numerically: $0.02601 \times 0.97399 \approx 0.02533$. The relation in (10) specifies the state equilibrium variance of the lepton sector. It will be shown later in the solar angle as the charged-lepton correction provided as: $\sin^2\theta_{12} = 1/3 - \alpha_l(1-\alpha_l)$, and in the reactor angle as the primary leptonic amplitude $\sin^2\theta_{13} = \alpha_l(1-\alpha_l) - \lambda^3/3$.

iii. *Relative Magnitude Compared to α_q.* We find $\alpha_l < \alpha_q$ because $\mathcal{C}_\ell = 1/2 < \mathcal{C}_q = 7/6$, since the compliant lepton sector places the small-perturbation component α_l closer to zero than the quark-sector parameter α_q.

iv. *Leptonic Weinberg Angle.* We can define the Leptonic-Weinberg angle θ_L by the relation $\alpha_l = \tan^2(\theta_L/2)$ as the lepton-sector analogue of the Weinberg angle. We find $\theta_L \approx 18.3^\circ$, reflecting the leptonic electroweak equilibrium at $\mathcal{C}_\ell = 1/2$.

The relative magnitudes of the equilibrium mixing-weights and the mixing variance, as represented in the unified mixing equilibrium condition for the quark and lepton sectors, are shown in Fig. 2. The quadratic equilibrium condition $\alpha_i(1-\alpha_i) = \mathcal{C}_i\lambda^2$ defines the equilibrium point on the underlying generic variance trajectory bounded by an upper stability threshold at $\alpha = 0.5$ corresponding to a peak variance of 1/4. This critical limit is never reached by either sector; beyond it, real solutions would cease to exist and the flavour state destabilises. Both sectors, however, operate with small parameters, with leptons at $\alpha_\ell \approx 0.026$ and quarks at $\alpha_q \approx 0.063$, residing safely on the lower slope of the curve, far below the critical ceiling. Quarks sit relatively higher up this slope (≈ 2.5 times that of leptons), imparting a stiffer vacuum response and a stronger restorative constraint, yielding a lower equilibrium retention-weight and a higher equilibrium mixing-weight compared to leptons, enforcing hierarchical suppression of mixing amplitudes. The lower equilibrium mixing-weight of the lepton sector represents a compliant configuration resulting in large mixing angles.

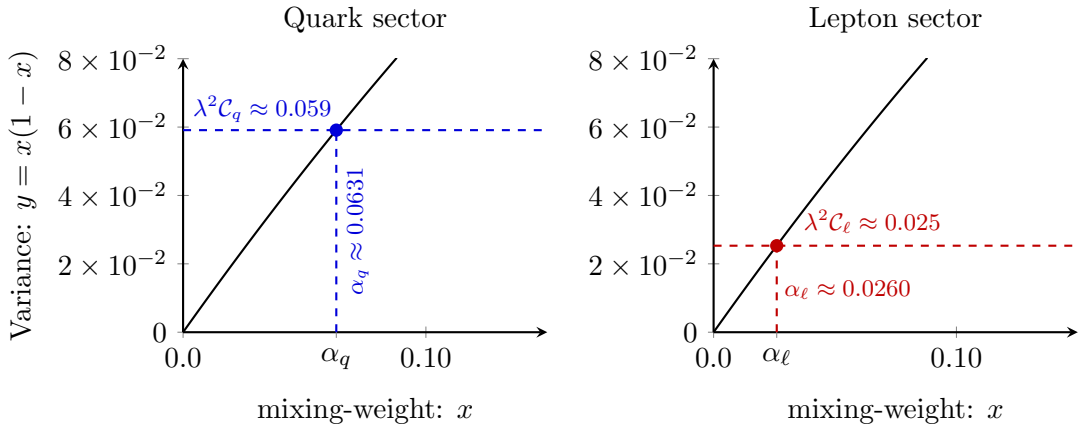


Figure 2: The solutions of the mixing equilibrium condition for the two sectors. The plot is the variance $y = x(1-x)$. The horizontal line is the equilibrium variance $\lambda^2 \mathcal{C}_i$. The intersection gives the mixing weight α_i at the point of equilibrium.

2.5 Charge-Neutral Isospin Considerations and Mixing Mechanism

The charge-neutral location ($Q = 0$) of a left-handed fermion occurs at the isospin value $T_3^{(0)}$ satisfying $Q = T_3^{(0)} + D_\ell/2 = 0$:

$$T_3^{(0)} = -\frac{D_\ell}{2} = -\frac{B-L}{2}. \tag{12}$$

Table 4 and Fig. 3 describe the charge and weak isospin projection behaviour in both sectors.

A remarkable fact to note in Fig. 3 is that phase traversal happens in the lower semicircle, representing the phase changing from 0° to 180° and passing through 270°, which corresponds to the maximal CP-violation phase. The key consequence that follows from the isospin displacements $\Delta T_3 = 0$ and $\Delta T_3 = -1$ can be analysed as follows:

(a) **Unsuppressed neutrino mixing.** Because $\Delta T_3 = 0$, all three neutrino mass eigenstates are chirally equivalent with respect to the $Q = 0$ configuration. In the absence of any other suppression, the neutrino mass eigenstate wavefunction distributes with equal amplitude $1/\sqrt{N_g}$ across all $N_g = 3$ generations, forming the tribimaximal democratic baseline [12, 14]. This large solar mixing thus arises from native chiral equivalence.

(b) **Charged-lepton weak isospin modification on solar mixing.** The neutrino must traverse $\Delta T_3 = -1$ from $T_3 = +1/2$ to $T_3 = -1/2$ to acquire the $Q = -1$ charge state at $T_3 = -1/2$. This traversal in weak isospin space suppresses the neutrino mixing by reducing $\sin^2 \theta_{12}$ below its tribimaximal value.

Table 4: Charge-neutral point ($Q = 0$) in the weak isospin space of the quark and lepton sectors.

Sector	$T_3^{(0)}$	$\theta_0 = \arccos(2T_3^{(0)})$	$\Delta T_3^{(\text{lighter})}$	$\Delta T_3^{(\text{heavier})}$
Quarks	$-1/6$	$\approx 109.47°$	$2/3$ (u_L)	$1/3$ (d_L)
Leptons	$+1/2$	$0°$	0 (ν_L)	1 (e_L^-)

θ_0 is the angular position on the isospin circle; $\Delta T_3^{(\nu,d)}$ is the isospin displacement of the lighter doublet from θ_0.

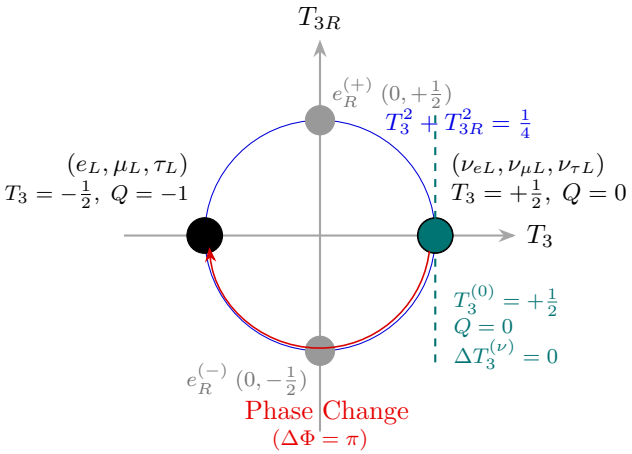


Figure 3: Static representation of the leptonic weak isospin space on the invariant Casimir circle $T_3^2+T_{3R}^2 = \frac{1}{4}$. It shows that the discrete phase rotation arc ($\Delta\Phi = \pi$) establishes the connection between the neutral neutrino doublet member ($T_3 = +1/2, Q = 0$) and its charged-lepton counterpart ($T_3 = -1/2, Q = -1$).

Table 4 shows the contrast between the charge-neutral weak isospin points $T_3^{(0)}$ in the quark and lepton sectors and the resulting changes in the isospin projection of the lighter doublet member from that neutral point. The physically decisive entry is $\Delta T_3 = 0$ for leptons: the lepton neutral point coincides exactly with the neutrino position on the isospin circle ($\theta_0 = 0°$), so neutrinos experience zero isospin barrier to inter-generation mixing. By contrast, the quark neutral point sits at $\theta_0 \approx 109.5°$, displaced from both the up-type and down-type quark positions, which explains the geometric origin of the small Cabibbo angle.

While Fig. 3 maps these configurations to the static weak isospin projection space, the physical mechanism of flavour transition follows a dynamic pipeline to execute these transformations. To illustrate this mechanism, Fig. 4 maps a generic charged-current flow to quantum number evolution in real time. During a flavour-changing interaction, the state vector enters via a source mixing matrix ($U^\dagger$) fixed at a definite weak isospin state ($T_{3L} = +1/2$). As the state vector transits through the propagation channel, it experiences a continuous phase rotation mediated by the underlying $SU(2)_L$ current generators (σ_i). At the exact spatial midpoint of this path ($\Delta\phi \to 270°$), the expectation value of the weak isospin crosses zero ($\langle T_{3L}\rangle \to 0$), demonstrating the continuous evolution of the wave amplitude before it acquires its final charged state ($T_{3L} = -1/2$) at the terminal projection matrix (U). This sequential framework demonstrates how any elementary flavour transition is fundamentally a joint evolution of charge coordinates, weak isospin projection coordinates, and spatial phase shifts.

3 Formulation of the PMNS Mixing Angles

3.1 The PMNS Matrix

Neutrino flavour eigenstates $|\nu_\alpha\rangle$ with $\alpha = e, \mu, \tau$ are not identical to the mass eigenstates $|\nu_i\rangle$ with $i = 1, 2, 3$. The two bases are related by a unitary matrix U,

$$|\nu_\alpha\rangle = \sum_{i=1}^{3} U_{\alpha i}\, |\nu_i\rangle. \tag{13}$$

The matrix U is called the PMNS matrix. In the standard parametrisation adopted by the PDG, U is written as the product of three rotations,

$$U = R_{23}(\theta_{23})\, U_{13}(\theta_{13}, \delta)\, R_{12}(\theta_{12}), \tag{14}$$

where R_{ij} denotes a rotation in the ij plane and δ is the CP-violating phase. The three real parameters θ_{12}, θ_{23}, and θ_{13} are the mixing angles. The corresponding individual rotations are

$$R_{12} = \begin{pmatrix} c_{12} & s_{12} & 0 \\ -s_{12} & c_{12} & 0 \\ 0 & 0 & 1 \end{pmatrix}, \quad R_{23} = \begin{pmatrix} 1 & 0 & 0 \\ 0 & c_{23} & s_{23} \\ 0 & -s_{23} & c_{23} \end{pmatrix}, \quad U_{13} = \begin{pmatrix} c_{13} & 0 & s_{13}e^{-i\delta} \\ 0 & 1 & 0 \\ -s_{13}e^{i\delta} & 0 & c_{13} \end{pmatrix}, \tag{15}$$

where the shorthand notation refers to:

$$s_{ij} = \sin\theta_{ij}, \qquad c_{ij} = \cos\theta_{ij}. \tag{16}$$

The full PMNS matrix is the product $U = R_{23}U_{13}R_{12}$, written explicitly as

$$U = \begin{pmatrix} c_{12}c_{13} & s_{12}c_{13} & s_{13}e^{-i\delta} \\ -s_{12}c_{23} - c_{12}s_{23}s_{13}e^{i\delta} & c_{12}c_{23} - s_{12}s_{23}s_{13}e^{i\delta} & s_{23}c_{13} \\ s_{12}s_{23} - c_{12}c_{23}s_{13}e^{i\delta} & -c_{12}s_{23} - s_{12}c_{23}s_{13}e^{i\delta} & c_{23}c_{13} \end{pmatrix}. \tag{17}$$

The squared moduli of the matrix elements define the array

$$|U|^2 = \begin{pmatrix} |U_{e1}|^2 & |U_{e2}|^2 & |U_{e3}|^2 \\ |U_{\mu 1}|^2 & |U_{\mu 2}|^2 & |U_{\mu 3}|^2 \\ |U_{\tau 1}|^2 & |U_{\tau 2}|^2 & |U_{\tau 3}|^2 \end{pmatrix}. \tag{18}$$

The unitarity condition constrains the sum of the squared moduli in each row and each column of this matrix to unity.

3.2 The Solar Angle (θ_{12})

The solar mixing angle θ_{12} describes the rotation between the flavour basis $\{|\nu_e\rangle, |\nu_\mu\rangle\}$ and the mass basis $\{|\nu_1\rangle, |\nu_2\rangle\}$,

$$\begin{pmatrix} |\nu_e\rangle \\ |\nu_\mu\rangle \end{pmatrix} = \begin{pmatrix} \cos\theta_{12} & \sin\theta_{12} \\ -\sin\theta_{12} & \cos\theta_{12} \end{pmatrix} \begin{pmatrix} |\nu_1\rangle \\ |\nu_2\rangle \end{pmatrix}. \tag{19}$$

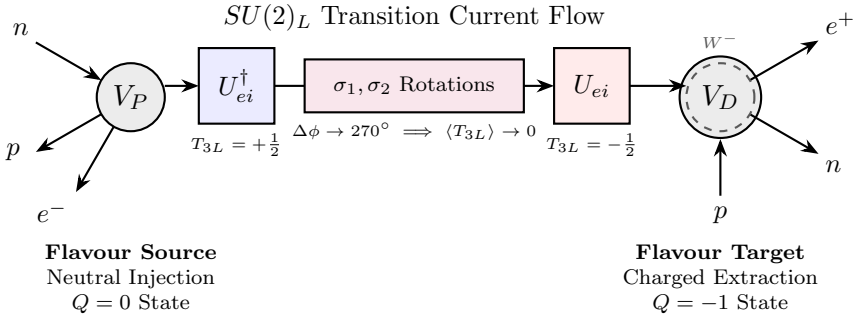


Figure 4: Operational example of charged-current lepton mixing. The pipeline tracks the state across weak isospin space, mapping a continuous rotation through the $SU(2)_L$ generators where phase changes ($\Delta\phi$), charge modifications (Q), and isospin shifts (T_{3L}) advance simultaneously toward the target.

The off-diagonal coefficient $\sin\theta_{12}$ governs the transition channel. It is the mixing amplitude between the flavour and mass bases. The diagonal coefficient $\cos\theta_{12}$ governs the survival channel. It is the retention amplitude of the primary state.

An electron neutrino produced at a charged-current vertex is the superposition

$$|\nu_e\rangle = \cos\theta_{12}\,|\nu_1\rangle + \sin\theta_{12}\,|\nu_2\rangle. \tag{20}$$

The mass eigenstates propagate through the vacuum. They accumulate distinct phases because they have different masses during oscillation. The phase difference over a baseline L is

$$\Delta\phi = \frac{\Delta m^2_{21} L}{2E}, \tag{21}$$

where E is the neutrino energy and $\Delta m^2_{21} \equiv m^2_2 - m^2_1$. At the detection vertex, the muon neutrino flavour state is

$$|\nu_\mu\rangle = -\sin\theta_{12}\,|\nu_1\rangle + \cos\theta_{12}\,|\nu_2\rangle. \tag{22}$$

The transition probability is the squared projection

$$P(\nu_e \to \nu_\mu) = |\langle\nu_\mu|\nu(L)\rangle|^2 = \sin^2(2\theta_{12})\sin^2\left(\frac{\Delta m^2_{21} L}{4E}\right). \tag{23}$$

The electron-neutrino survival probability is the complement

$$P(\nu_e \to \nu_e) = 1 - \sin^2(2\theta_{12})\sin^2\left(\frac{\Delta m^2_{21} L}{4E}\right). \tag{24}$$

3.2.1 Baseline Value

The baseline value of the solar angle is fixed by the democratic limit. In the democratic limit, all three generations contribute with equal weight. The baseline state is the equal-amplitude superposition

$$|\nu^{(0)}\rangle = \frac{1}{\sqrt{N_g}}\sum_{i=1}^{N_g}|\nu_i\rangle = \frac{1}{\sqrt{3}}\left(|\nu_1\rangle + |\nu_2\rangle + |\nu_3\rangle\right), \tag{25}$$

where $N_g = 3$. Each generation carries the amplitude $1/\sqrt{3}$. The Born-rule probability for each generation is

$$P_i^{(0)} = \frac{1}{N_g} = \frac{1}{3}. \tag{26}$$

The normalization is preserved, so that

$$\sum_{i=1}^{3} P_i^{(0)} = 3 \times \frac{1}{3} = 1. \tag{27}$$

The baseline mixing probability is therefore

$$\sin^2\theta_{12}^{(0)} = \frac{1}{N_g} = \frac{1}{3}. \tag{28}$$

The corresponding angle is

$$\theta_{12}^{(0)} = \arcsin\left(\frac{1}{\sqrt{3}}\right) \approx 35.26^\circ. \tag{29}$$

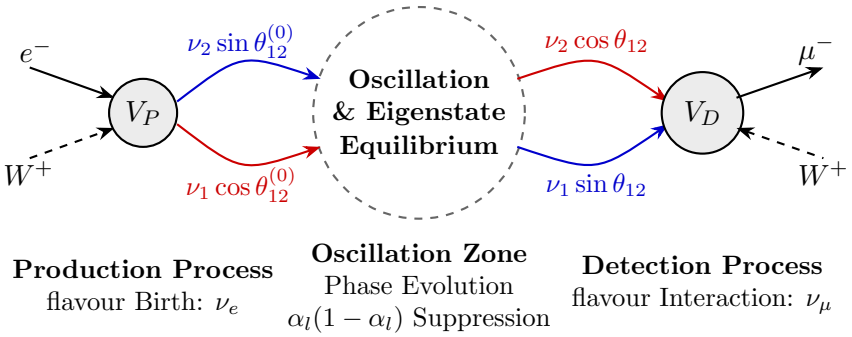


Figure 5: Solar neutrino oscillation mechanism incorporating localized amplitude suppression.

The baseline connects to the electroweak quantum numbers through the neutrino isospin projection

$$T_3^{(\nu_L)} = +\frac{1}{2}, \qquad Q_\nu = 0. \tag{30}$$

The neutrino lies at the charge-neutral point of the weak-isospin doublet. Its isospin displacement vanishes, $\Delta T_3 = 0$. This connects the baseline to the gauge structure.

3.2.2 Charged-Current Suppression

The mixing mechanism is depicted in the schematic diagram in Fig. 5. The electron neutrino is produced at the production vertex V_P as a linear combination of mass eigenstates ν_1 and ν_2 weighted by $\cos\theta_{12}$ and $\sin\theta_{12}$, respectively. The two mass eigenstates are shown to propagate from the production vertex to the detection vertex.

While transiting to the detection vertex V_D through the quantum oscillation zone, the eigenstates accumulate relative quantum phases due to their mass splitting. At the detection vertex V_D, the evolved state is projected onto the orthogonal muon neutrino flavour basis, effectively transposing the projection amplitudes to yield the final transition probability. The intervening vacuum modifies the amplitudes of the mass eigenstates ν_1 and ν_2. Moreover, the transition amplitude is suppressed by the state equilibrium variance $\delta = \alpha_l(1-\alpha_l)$, where $1-\alpha_l \approx \sin\delta_{\rm CP}^{\rm PMNS}$.

In the three-state flavour mix, the first-generation electron channel exhibits behaviour distinct from the heavily blended muon and tau channels. Empirically, the electron neutrino flavour eigenstate maps onto the primary mass eigenstate with a dominating probability of approximately 67%. Consequently, rather than actively driving larger flavour rotations, the electron channel behaves as an isolated channel that is firmly anchored to the baseline.

Therefore, we hypothesize here that, in the solar sector, the electron is silent spectator without changing the baseline amplitudes of $\cos\theta_{12}^{(0)}$ and $\sin\theta_{12}^{(0)}$ for the first and second mass eigenstate ν_1 and ν_2, respectively. The muon other hand favours the second mass eigenstate ν_2, so that the effective solar angle is lower than the democratic baseline, and the mixing process reduces the transition amplitude. The charged-current interaction therefore reduces the transition amplitude by the amount equal to the lepton-sector *equilibrium mixing variance*:

$$\delta = \alpha_l(1-\alpha_l). \tag{31}$$

Using it with the baseline value in (28), the effective solar angle can be obtained as:

$$\sin^2\theta_{12} = \sin^2\theta_{12}^{(0)} - \delta = \frac{1}{3} - \alpha_l(1-\alpha_l). \tag{32}$$

The variance is provided by the sector mixing equilibrium condition in (10), as:

$$\alpha_l(1-\alpha_l) = C_l\lambda^2 = \frac{1}{2}\lambda^2 = \frac{1}{4\pi^2}.$$

Numerically, this is evaluated to yield:

$$\alpha_l(1-\alpha_l) \approx 0.025330, \tag{33}$$

$$\sin^2\theta_{12} = 0.333333 - 0.025330 = 0.308003. \tag{34}$$

The effective value of the mixing angle can thus be derived as:

$$\theta_{12} = \arcsin\left(\sqrt{0.308003}\right) \approx 33.71^\circ. \tag{35}$$

Benchmarking against the global three-flavour oscillation analysis framework (NuFIT 6.0) [25] gives the standard baseline comparison parameter:

$$\sin^2\theta_{12}^{(\mathrm{PDG})} = 0.307 \pm 0.012 \implies \theta_{12} = (33.65 \pm 0.75)^\circ. \tag{36}$$

The effective solar angle derived from the proposed model agrees well with the global empirical average, converging within the minor 0.08σ confidence.

3.3 The Atmospheric Angle (θ_{23})

The atmospheric rotation between the flavour basis (ν_μ, ν_τ) and the mass basis (ν_2, ν_3) is given by the standard planar matrix formulation:

$$\begin{pmatrix}\nu_\mu\\ \nu_\tau\end{pmatrix} = \begin{pmatrix}\cos\theta_{23} & \sin\theta_{23}\\ -\sin\theta_{23} & \cos\theta_{23}\end{pmatrix}\begin{pmatrix}\nu_2\\ \nu_3\end{pmatrix}. \tag{37}$$

The off-diagonal coefficient $\sin\theta_{23}$ governs the transition channel, whereas the diagonal coefficient $\cos\theta_{23}$ dictates the survival channel. The four entries of the rotation matrix represent the projection amplitudes, whose squared moduli define the respective transition probabilities:

$$|\langle\nu_\mu|\nu_2\rangle|^2 = \cos^2\theta_{23}, \qquad |\langle\nu_\mu|\nu_3\rangle|^2 = \sin^2\theta_{23}, \tag{38}$$

$$|\langle\nu_\tau|\nu_2\rangle|^2 = \sin^2\theta_{23}, \qquad |\langle\nu_\tau|\nu_3\rangle|^2 = \cos^2\theta_{23}. \tag{39}$$

3.3.1 Baseline Value

The $\mu \leftrightarrow \tau$ flavour exchange is nearly symmetric under standard exchange operations, suggesting the two flavour configurations are equally populated in the unperturbed limit. Consequently, the mass eigenstates ν_2 and ν_3 carry matching mixing amplitudes:

$$\cos^2\theta_{23}^{(0)} \approx \sin^2\theta_{23}^{(0)}. \tag{40}$$

Taking the exact symmetric limit,

$$\cos^2\theta_{23}^{(0)} = \sin^2\theta_{23}^{(0)}. \tag{41}$$

This fixes the baseline, unperturbed maximal mixing intensity at:

$$\sin^2\theta_{23}^{(0)} = \frac{1}{2}. \tag{42}$$

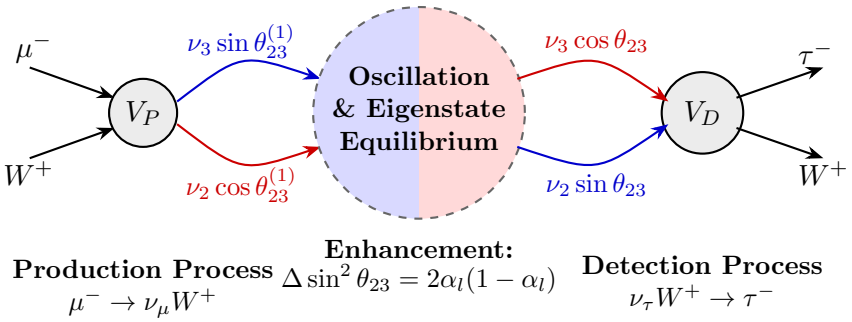


Figure 6: The atmospheric neutrino mixing mechanism.

3.3.2 Charged-Current Amplitude Enhancement

The charged-current weak interaction breaks the underlying baseline flavour symmetry. The production vertex establishes the initial flavour state as a superposition of mass eigenstates, while the detection vertex projects the evolved state onto the final flavour state. Between these interaction boundaries, the central eigenstate equilibrium zone modifies the mixing amplitudes. This structural modification is fixed globally by the invariant lepton-sector constraint:

$$\alpha_l(1-\alpha_l) = \frac{1}{4\pi^2}. \tag{43}$$

The mixing mechanism is illustrated in the schematic in Fig. 6. The production vertex V_P creates the initial flavour configuration, while the detection vertex V_D projects out the modified configuration as a tau neutrino flavour state.

The production process maps to the vertex $\mu^- \to \nu_\mu W^+$, while the detection process maps to the vertex $\nu_\tau W^+ \to \tau^-$. The muon neutrino ν_μ is born at the production vertex V_P, sends the two mass eigenstates ν_2 and ν_3 with the baseline amplitudes. During propagation, the intervening eigenstate equilibrium zone modifies the amplitudes of the two mass fields symmetrically by the mixing equilibrium variance amount $\alpha_l(1-\alpha_l)$.

In the solar sector, we hypothesize that, the muon favours the second mass eigenstate ν_2, reducing the effective solar angle to lower than the democratic baseline. In the atmospheric sector, we hypothesize that, the muon favours the third mass eigenstate ν_3, while the tau favours the second mass eigenstate ν_2, increasing the atmospheric angle over the democratic baseline and the transition amplitude at each process by the equilibrium variance $\alpha_l(1-\alpha_l)$.

The production process dynamically sets the initial mixing angle to $\theta_{23}^{(0)} = 45°$. Vacuum propagation subsequently enhances the mixing; and modifies the configuration to an intermediate angle, $\theta_{23}^{(1)}$ to represent the enhancement of transition amplitude over the baseline value 1/2, such that:

$$\sin^2\theta_{23}^{(1)} = \sin^2\theta_{23}^{(0)} + \alpha_l(1-\alpha_l) = \frac{1}{2} + \alpha_l(1-\alpha_l). \tag{44}$$

Subsequently, the detection process projects this modified wave function at the target vertex, increasing the effective mixing intensity further to $\sin^2\theta_{23}$:

$$\sin^2\theta_{23} = \sin^2\theta_{23}^{(1)} + \alpha_l(1-\alpha_l) = \frac{1}{2} + 2\alpha_l(1-\alpha_l). \tag{45}$$

Because these interactions could be viewed as affecting sequentially, the net enhancement is precisely

twice the single-stage equilibrium variance as[1]:

$$\Delta \sin^2 \theta_{23} = 2\alpha_l(1-\alpha_l) = \lambda^2. \tag{46}$$

Using the numerical value of equilibrium variance $\alpha_l(1-\alpha_l) \approx 0.025330$ we get:

$$\sin^2 \theta_{23} = 0.500000 + 2(0.025330) = 0.550660, \tag{47}$$

$$\theta_{23} = \arcsin\left(\sqrt{0.550660}\right) \approx 47.91^\circ. \tag{48}$$

To test the accuracy of this prediction, we benchmark the result against the global three-flavour neutrino oscillation data fits (NuFIT 6.0) [25], which report the preferred value for normal mass hierarchies:

$$\sin^2 \theta_{23}^{(\mathrm{PDG})} = 0.563^{+0.018}_{-0.024} \implies \theta_{23} = \left(48.62^{+1.05}_{-1.35}\right)^\circ. \tag{49}$$

The proposed parameter-free prediction of $\sin^2 \theta_{23} \approx 0.5507$ is found to be within the empirical 1σ window, breaking the octant symmetry in favour of the second octant ($\sin^2 \theta_{23} > 0.5$) at 0.51σ difference.

3.4 The Reactor Angle (θ_{13})

The reactor mixing angle θ_{13} parametrises the non-adjacent, cross-generational overlap between the first-generation flavour field (ν_e) and the third mass eigenstate (ν_3). In the standard three-flavour framework, this localized boundary mapping corresponds to the isolated $1 \leftrightarrow 3$ sector matrix:

$$R_{13} = \begin{pmatrix} \cos\theta_{13} & 0 & \sin\theta_{13} \\ 0 & 1 & 0 \\ -\sin\theta_{13} & 0 & \cos\theta_{13} \end{pmatrix}, \tag{50}$$

where the element $U_{e3} = \sin\theta_{13}$ dictates the static projection amplitude.

Reactor experiments however track electron antineutrino disappearance via the clean survival channel $\bar{\nu}_e \to \bar{\nu}_e$, ensuring the flavour eigenstate remains identical at both boundaries. Consequently, we explicitly do not model a complete, macroscopic flavour appearance oscillation to the third generation ($\bar{\nu}_\tau$) during vacuum flight representing (50). We consider the first row of the rotation matrix, which consists of purely real spatial coefficients and behaves as a single-channel current, completely delinked from the atmospheric angle θ_{23} and the Dirac CP phase δ_{PMNS}. The angle θ_{13} operates as a static geometric parameter tracking the overlap between the first-generation flavour field (ν_e) and the third mass eigenstate (ν_3). The flavour production and detection in this isolated tracking pipeline is shown in Fig. 7.

The core physical timeline maps these coupled mechanisms across three explicit stages:
The Production Process: The electron anti-neutrino $\bar{\nu}_e$ is born at the production vertex V_P via a standard beta decay profile ($n \to p + e^- + \bar{\nu}_e$). The state vector initializes against a vanishing baseline value at the source, where $\theta_{13}^{(0)} \approx 0$. However, the production process triggers a positive local enhancement to the initial coupling space equal to the localized equilibrium variance, resulting the amplitude:

$$\sin^2 \theta_{13}^{(1)} = \alpha_l(1-\alpha_l). \tag{51}$$

Because the direct unperturbed baseline channel is closed ($\sin^2 \theta_{13}^{(0)} \to 0$) in the reactor scale, this state equilibrium variance acts as the sole generator initializing the mass eigenstate amplitude

[1]Note that neither interaction vertex involves the electron channel. The first lepton generation does not participate in this channel, ensuring the structural enhancement undergoes no dilution from cross-flavour branching ratios.

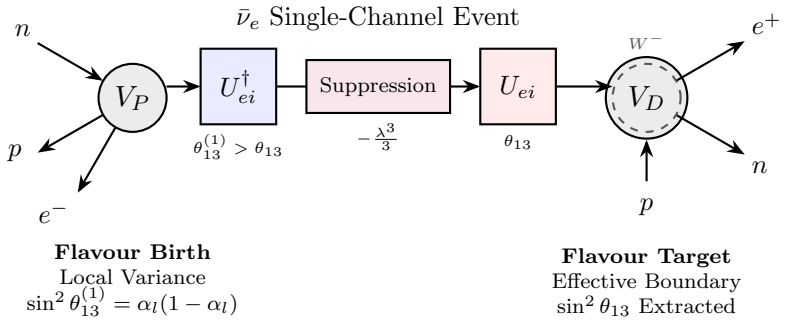


Figure 7: The reactor process mapped as a sequential single-channel event.

at birth. The $\bar{\nu}_e$ state is therefore born with a nonzero ν_3 amplitude. The flavour state is the superposition,

$$|\bar{\nu}_e\rangle = \cos\theta_{13}^{(1)}\,|\bar{\nu}_1\rangle + \sin\theta_{13}^{(1)}\,|\bar{\nu}_3\rangle. \tag{52}$$

Skip-Generation Suppression: The production process being associated with the amplitude distribution across the generation gap with the third mass eigenstate is accompanied by a cross-generational damping factor:

$$-\frac{\lambda^3}{3} \approx -0.00380. \tag{53}$$

This suppression term $(-\lambda^3/3)$ can viewed as the back-reaction the state equilibrium variance enhancement of (51) in the production mechanism.

The Detection Process: The remaining amplitude is projected at the detection vertex V_D via standard low-energy inverse beta decay ($\bar{\nu}_e + p \to e^+ + n$), mediated internally by the W^- boson current. The net physically observed reactor mixing angle emerges dynamically from the combination of the production enhancement and the cross-generation suppression:

$$\sin^2\theta_{13} = \sin^2\theta_{13}^{(0)} + \alpha_l(1-\alpha_l) - \frac{\lambda^3}{3}. \tag{54}$$

Imposing the limit where the unperturbed initial geometric baseline vanishes ($\sin^2\theta_{13}^{(0)} \to 0$), the absolute parameter-free expression reduces cleanly to:

$$\sin^2\theta_{13} = \frac{\lambda^2}{2} - \frac{\lambda^3}{3}. \tag{55}$$

Evaluating this expression using the universal fermion mixing constant ($\lambda \approx 0.225079$) yields the following numerical outputs:

$$\sin^2\theta_{13} \approx 0.025330 - 0.003800 = 0.021530, \tag{56}$$

$$\theta_{13} = \arcsin\sqrt{0.021530} \approx 8.44^\circ. \tag{57}$$

Benchmarking this derived parameter against the modern global neutrino oscillation analysis world average [NuFIT 6.0], where $\sin^2\theta_{13}^{(\mathrm{exp})} = 0.02203 \pm 0.00056$, demonstrates strong numerical agreement at the 0.89σ level.

3.5 The Dirac CP Violation Phase and Leptonic Jarlskog Invariant

We assume here that the neutrino mass matrix is strictly real with its charge-neutral fields ($Q = 0$) in the absence of any charged lepton current as shown in Fig. 3. It undergoes transformation due to the weak interaction during flavour mixing. The complex CP-violating phase is dynamically absorbed by the neutrino via the unitary transformation. Relative to the CP-conserving neutrino baseline, it undergoes a relative phase inversion in the presence of the charged lepton. Accordingly, the unperturbed reference configuration of the neutrino mass eigenstates is characterized by a phase baseline of $\delta = 0$ which is changed to $\delta = -\pi$ (-180°) in the final state, representing the standard CP-conserving reflection. As shown in Fig. 3, the neutrino state passes in a clockwise direction in weak isospin space from the $T_3 = +1/2, Q = 0, \delta = 0$ configuration to the $T_3 = -1/2, Q = -1, \delta = -\pi$ configuration, passing through the $T_3 = 0, Q = -1/2, \delta = -\pi/2 \equiv 3\pi/2$ midpoint at the maximal CP-violation phase.

3.5.1 Determination of Leptonic Dirac CP Phases

The state function representing the mixing of active flavour states under mixing equilibrium conditions is given by:

$$|\Psi\rangle = \sqrt{\alpha_l}\,|0\rangle + \sqrt{1-\alpha_l}\,e^{i\phi_{\rm CP}}\,|1\rangle, \tag{58}$$

where $|0\rangle$ and $|1\rangle$ denote the orthogonal basis eigenstates corresponding to active flavour states, and $\phi_{\rm CP}$ represents the relative phase. The equilibrium mixing-weight α_l and retention-weight $(1-\alpha_l)$ are constrained by the lepton-sector mixing equilibrium condition $\alpha_l(1-\alpha_l) = \mathcal{C}_\ell\lambda^2 = \frac{1}{4\pi^2}$ given in (10), where $\mathcal{C}_\ell = 1/2$ is the sector coupling factor.

The equilibrium mixing-weight α_l and retention-weight $(1-\alpha_l)$ determine the phase components via the sine projection:

$$\delta_1 = \arcsin(\alpha_l) \quad \text{and} \quad \delta_2 = \arcsin(1-\alpha_l). \tag{59}$$

From (10), the numerical values are $\alpha_l \approx 0.02600664$ and $1-\alpha_l \approx 0.97399336$. Substituting these values yields:

$$\begin{aligned}\delta_1 &= \arcsin(\alpha_l) = \arcsin(0.02600664) \approx 0.02601 \text{ rad} \approx 1.49^\circ \quad \text{and}\\ \delta_2 &= \arcsin(1-\alpha_l) = \arcsin(0.97399336) \approx 1.33521 \text{ rad} \approx 76.90^\circ.\end{aligned} \tag{60}$$

The charged lepton mass eigenstates are not invariant under separate charge conjugation (C) or parity (P) transformations due to the chiral nature of the weak interaction. Based on the weak isospin representation derived from GMN, as shown in Fig. 3, the unperturbed reference configuration is defined at $\delta_0 = 0^\circ$ (or 360° for clockwise phase traversal on the lower semicircle), with a relative phase inversion at $\delta_0 = 180^\circ$ serving as the CP-conserving baseline. The phase components δ_1 and δ_2, derived directly from the mixing equilibrium conditions, specify the angular displacements from these baselines. Projecting these values yields the PMNS Dirac CP phases for the two neutrino mass orderings:

$$\delta^{\rm PMNS}_{\rm CP,\,NO} = 180^\circ + \delta_1 = 180^\circ + 1.49^\circ = 181.49^\circ, \tag{61}$$

$$\delta^{\rm PMNS}_{\rm CP,\,IO} = 360^\circ - \delta_2 = 360^\circ - 76.90^\circ = 283.10^\circ, \tag{62}$$

where the normal ordering phase corresponds to the 180° baseline via the forward path, and the inverted ordering phase corresponds to the reverse path in clockwise direction. Because these values are derived from closed-form analytical equilibrium relations without free parameters, they constitute strict, falsifiable predictions for upcoming long-baseline experiments; any measurement inconsistent with these specific projections falsifies the underlying relation between the mixing/retention-weights and the CP-violating phase.

The PMNS Dirac CP phases obtained in (61) and (62) are examined here to find possible agreement with the current global oscillation analyses (NuFIT 6.0).

Normal Ordering (NO): The equilibrium mixing-weight α_ℓ yields $\delta^{\rm PMNS}_{\rm CP,\,NO} = 180^\circ + \arcsin(\alpha_\ell) = 181.49^\circ$. Comparing it against the NO global best-fit value ($\delta^{\rm bfp}_{\rm CP} \simeq 197^\circ$ with a 1σ uncertainty envelope of 20.0°) we find:

$$\sigma^{\rm NO}_{\rm pull} = \frac{|181.49^\circ - 197.0^\circ|}{20.0^\circ} = \frac{15.51^\circ}{20.0^\circ} \approx 0.78\sigma. \tag{63}$$

Inverted Ordering (IO): The equilibrium retention-weight $(1-\alpha_\ell)$ yields $\delta^{\rm PMNS}_{\rm CP,\,IO} = 360^\circ - \arcsin(1-\alpha_l) = 283.10^\circ$. Comparing it against the IO global best-fit value ($\delta^{\rm bfp}_{\rm CP} \simeq 274^\circ$ with a 1σ uncertainty envelope of 25.0°) we find:

$$\sigma^{\rm IO}_{\rm pull} = \frac{|283.10^\circ - 274.0^\circ|}{25.0^\circ} = \frac{9.10^\circ}{25.0^\circ} \approx 0.36\sigma. \tag{64}$$

3.6 The Leptonic Jarlskog Invariant $J_{\rm CP}$

The Jarlskog rephasing-invariant measure of CP violation in the lepton sector is defined as:

$$J_{\rm CP} = \cos\theta_{12}\sin\theta_{12}\cos\theta_{23}\sin\theta_{23}\cos^2\theta_{13}\sin\theta_{13}\sin\delta^{\rm PMNS}_{\rm CP}. \tag{65}$$

Substituting the derived mixing values ($\sin^2\theta_{12} = 0.3080, \cos\theta_{12}\sin\theta_{12} \approx 0.46177$, $\sin^2\theta_{23} = 0.5507, \cos\theta_{23}\sin\theta_{23} \approx 0.49730$, $\sin^2\theta_{13} = 0.0215$, and $\cos^2\theta_{13}\sin\theta_{13} \approx 0.14363$) alongside the derived phases $\delta^{\rm PMNS}_{\rm CP,\,NO} = 181.49^\circ$ and $\delta^{\rm PMNS}_{\rm CP,\,IO} = 283.10^\circ$ yields:

NO Regime: $J^{\rm NO}_{\rm CP} = (0.46177) \times (0.49730) \times (0.14363) \times (-0.02601) \approx -0.000858.$

IO Regime: $J^{\rm IO}_{\rm CP} = (0.46177) \times (0.49730) \times (0.14363) \times (-0.97399) \approx -0.0321.$

Evaluated against global oscillation benchmarks (NuFIT 6.0) yields the explicit invariant pulls:

Normal Ordering (NO): Comparing $J^{\rm NO}_{\rm CP} = -0.000858$ against the NO global best-fit ($J^{\rm bfp}_{\rm CP} \approx -0.0050$ with a 1σ uncertainty of 0.0055) yields a residual of 0.004142, giving the explicit pull:

$$\sigma^{\rm NO}_{\rm pull} = \frac{|-0.000858 - (-0.0050)|}{0.0055} = \frac{0.004142}{0.0055} \approx 0.75\sigma. \tag{66}$$

Inverted Ordering (IO): Comparing $J^{\rm IO}_{\rm CP} = -0.0321$ against the IO global best-fit ($J^{\rm bfp}_{\rm CP} \approx -0.0330$ with a 1σ uncertainty of 0.0035) yields a residual of 0.0009, giving the explicit pull:

$$\sigma^{\rm IO}_{\rm pull} = \frac{|-0.0321 - (-0.0330)|}{0.0035} = \frac{0.0009}{0.0035} \approx 0.26\sigma. \tag{67}$$

Since these results are obtained by mapping the equilibrium mixing-weight and the equilibrium retention-weight to the sine projections of Dirac CP phase without free parameters, they are directly falsifiable by experimental disagreement under either mass ordering.

The ratio $|J^{\rm IO}_{\rm CP}/J^{\rm NO}_{\rm CP}| = 0.0321/0.000858 \approx 37$ is a parameter-free prediction of the equilibrium condition. It follows directly from the two-root structure of the mixing equilibrium condition: since $J \propto \sin\delta_{\rm CP}$, the ratio equals $\sin\delta_{\rm CP,IO}/\sin\delta_{\rm CP,NO} = (1-\alpha_\ell)/\alpha_\ell$. With $\alpha_\ell \approx 0.026$ and $1-\alpha_\ell \approx 0.974$, this gives $(1-\alpha_\ell)/\alpha_\ell \approx 37$. The IO branch therefore carries near-maximal leptonic CP violation, while the NO branch is near CP-conserving. This 37-fold ordering asymmetry is a sharp discriminant accessible to DUNE and Hyper-Kamiokande through the $\nu_\mu \to \nu_e$ appearance channel.

4 The Complete PMNS Matrix and Quark–Lepton Duality

The four mixing parameters and CP-violating phases derived in previous sections provide the necessary numerical inputs: $s_{12} \approx 0.5550$, $c_{12} \approx 0.8319$, $s_{23} \approx 0.7421$, $c_{23} \approx 0.6703$, $s_{13} \approx 0.1467$, $c_{13} \approx 0.9892$, $\delta^{\rm PMNS}_{\rm CP,NO} \approx 181.49°$, and $\delta^{\rm PMNS}_{\rm CP,IO} \approx 283.10°$. These inputs determine all the PMNS matrix elements evaluated across both mass orderings in the following subsections.

4.1 Normal Ordering PMNS Matrix and Element Evaluation

Using the evaluated trigonometric functions of the mixing angles and the CP-violating phase, the NO-branch PMNS matrix is computed as:

$$U^{\rm NO}_{\rm PMNS} = \begin{pmatrix} 0.8228 & 0.5490 & 0.1467\, e^{-i(181.49°)} \\ -0.2814 - 0.0024i & 0.6180 & 0.7340 \\ 0.4937 & -0.5628 & 0.6631 \end{pmatrix}. \tag{68}$$

Taking the moduli of the matrix elements produces:

$$|U^{\rm NO}_{\rm PMNS}| = \begin{pmatrix} 0.823 & 0.549 & 0.147 \\ 0.281 & 0.618 & 0.734 \\ 0.494 & 0.563 & 0.663 \end{pmatrix}. \tag{69}$$

To quantify the agreement under Normal Ordering, we compare each element against NuFIT 6.0 Normal Ordering best-fit values [25], propagating the 1σ uncertainties on the mixing angles and $\delta^{\rm NO}_{\rm CP}$ to obtain element-wise uncertainties via the statistical pull definition:

$$\text{Pull}_{ij} = \frac{|U^{\rm theory}_{ij}| - |U^{\rm NuFIT}_{ij}|}{\sigma_{{\rm NuFIT},ij}}. \tag{70}$$

Table 5 presents the element-by-element comparison for the NO-branch evaluation. Across all nine elements, the maximum pull is $1.53\,\sigma$ (at $|U_{\mu 3}|$ and $|U_{\tau 3}|$), with a mean absolute pull of $0.56\,\sigma$ and an RMS pull of $0.78\,\sigma$.

4.2 Inverted Ordering (IO) PMNS Matrix and Element Evaluation

Conversely, the equilibrium retention-weight ($(1-\alpha_\ell) \approx 0.9740$) is applicable to the Inverted Ordering regime, yielding the large CP-violating phase $\delta^{\rm PMNS}_{\rm CP,\,IO} \approx 283.10°$. The IO-branch PMNS matrix is computed as:

$$U^{\rm IO}_{\rm PMNS} = \begin{pmatrix} 0.8228 & 0.5490 & 0.1467\, e^{-i(283.10°)} \\ -0.3925 + 0.0882i & 0.5439 + 0.0588i & 0.7340 \\ 0.3934 + 0.0797i & -0.6298 + 0.0532i & 0.6631 \end{pmatrix}. \tag{71}$$

Taking the moduli of the matrix elements produces:

$$|U^{\rm IO}_{\rm PMNS}| = \begin{pmatrix} 0.823 & 0.549 & 0.147 \\ 0.402 & 0.547 & 0.734 \\ 0.401 & 0.632 & 0.663 \end{pmatrix}. \tag{72}$$

Table 6 presents the element-by-element comparison of all nine PMNS matrix moduli against NuFIT 6.0 Inverted Ordering best-fit values. Since no free parameters enter the theoretical values, every pull is a direct test of the analytical equilibrium formulation. Across all nine elements,

Table 5: Comparison of the analytically derived PMNS matrix element moduli against NuFIT 6.0 Normal Ordering (NO) best-fit values [25].

Element	Theoretical	NuFIT NO	σ_{NuFIT}	Pull (σ)
$\lvert U_{e1}\rvert$	0.823	0.8233	0.0071	-0.04
$\lvert U_{e2}\rvert$	0.549	0.5479	0.0107	$+0.10$
$\lvert U_{e3}\rvert$	0.147	0.1483	0.0024	-0.68
$\lvert U_{\mu1}\rvert$	0.281	0.2780	0.0350	$+0.09$
$\lvert U_{\mu2}\rvert$	0.618	0.6120	0.0280	$+0.21$
$\lvert U_{\mu3}\rvert$	0.734	0.7519	0.0117	-1.53
$\lvert U_{\tau1}\rvert$	0.494	0.5100	0.0320	-0.50
$\lvert U_{\tau2}\rvert$	0.563	0.5520	0.0260	$+0.38$
$\lvert U_{\tau3}\rvert$	0.663	0.6424	0.0137	$+1.51$
Maximum |Pull|				1.53
Mean |Pull|				0.56
RMS Pull				0.81

Table 6: Comparison of the analytically derived PMNS matrix element moduli against NuFIT 6.0 Inverted Ordering (IO) best-fit values [25].

Element	Theoretical	NuFIT IO	σ_{NuFIT}	Pull (σ)
$\lvert U_{e1}\rvert$	0.823	0.8233	0.0071	-0.04
$\lvert U_{e2}\rvert$	0.549	0.5479	0.0107	$+0.10$
$\lvert U_{e3}\rvert$	0.147	0.1483	0.0024	-0.68
$\lvert U_{\mu1}\rvert$	0.402	0.3783	0.0391	$+0.61$
$\lvert U_{\mu2}\rvert$	0.547	0.5400	0.0291	$+0.24$
$\lvert U_{\mu3}\rvert$	0.734	0.7519	0.0117	-1.52
$\lvert U_{\tau1}\rvert$	0.401	0.4233	0.0352	-0.63
$\lvert U_{\tau2}\rvert$	0.632	0.6388	0.0249	-0.27
$\lvert U_{\tau3}\rvert$	0.663	0.6424	0.0137	$+1.51$
Maximum |Pull|				1.52
Mean |Pull|				0.62
RMS Pull				0.78

Table 7: Summary of analytic PMNS predictions vs. global fits (NuFIT / PDG) for both Normal and Inverted Orderings.

Observable	Analytic formula	Predicted	PDG / NuFIT Global Fit
$\sin^2\theta_{12}$	$\frac{1}{3} - \alpha_l(1-\alpha_l)$	0.3080	0.307 ± 0.012 ($+0.08\sigma$)
$\sin^2\theta_{13}$	$\alpha_l(1-\alpha_l) - \frac{\lambda^3}{3}$	0.0215	0.0220 ± 0.0007 (-0.89σ)
$\sin^2\theta_{23}$	$\frac{1}{2} + 2\alpha_l(1-\alpha_l) = \frac{1}{2} + \lambda^2$	0.5507	0.563 ± 0.024 (NO, -0.51σ)
$\delta^{\rm PMNS}_{\rm CP,NO}$	$180^\circ + \arcsin(\alpha_l)$	181.49°	$(197 \pm 20)^\circ$ NO (-0.78σ)
$\delta^{\rm PMNS}_{\rm CP,IO}$	$360^\circ - \arcsin(1-\alpha_l)$	283.10°	$(274 \pm 25)^\circ$ IO ($+0.36\sigma$)
$J^{\ell}_{\rm CP}$ (NO)	$s_{12}c_{12}s_{23}c_{23}s_{13}c_{13}^2 \sin\delta_{\rm CP,NO}$	-0.000858	-0.0050 ± 0.0055 NO ($+0.75\sigma$)
$J^{\ell}_{\rm CP}$ (IO)	$s_{12}c_{12}s_{23}c_{23}s_{13}c_{13}^2 \sin\delta_{\rm CP,IO}$	-0.0321	-0.0330 ± 0.0035 IO ($+0.26\sigma$)

the maximum pull is $1.52\,\sigma$ (at $|U_{\mu 3}|$ and $1.51\,\sigma$ at $|U_{\tau 3}|$, tracing to the second-third sector with $\sin^2\theta_{23} = 0.5507$ vs. NuFIT IO best-fit 0.578), with a mean absolute pull of $0.62\,\sigma$ and an RMS pull of $0.81\,\sigma$.

Table 7 is a comprehensive summary of analytical expressions and values calculated using the expressions, consolidating the PMNS observables for *both Normal Ordering and Inverted Ordering*, which include the three universal mixing angles alongside the ordering-specific Dirac CP phases and Jarlskog invariants. Each entry shows the closed-form analytic formula and its comparison against NuFIT 6.0 / PDG global data, demonstrating that the analytical equilibrium formulation successfully reproduces the complete leptonic mixing structure across both branches without free parameters. Evaluating the inner products confirms that the analytically derived PMNS matrices for both mass orderings satisfy row and column unitarity to better than the 10^{-4} level, demonstrating that the analytical equilibrium framework strictly preserves probability conservation across all generations.

4.3 Unitarity of the Derived PMNS Matrices

Unitarity is a fundamental requirement for any physically admissible mixing matrix [1, 8]. It ensures probability conservation across flavour detection channels ($UU^\dagger = I_3$) and completeness across mass eigenstates ($U^\dagger U = I_3$). To verify that our closed-form expressions satisfy these conditions, we construct the complex PMNS matrices for both NO and IO orderings using the derived mixing angles ($\theta_{12}, \theta_{23}, \theta_{13}$) and CP phases ($\delta_{\rm CP}$). We have checked the unitarity across the following three complementary quantitative metrics:

i. *Diagonal Deviations:* The absolute departures of row and column sums from unity, $|\sum_j |U_{ij}|^2 - 1|$ and $|\sum_i |U_{ij}|^2 - 1|$, are computed using the values of matrix elements and are detailed in Table 8.

ii. *Off-Diagonal Orthogonality:* The inner products between distinct rows ($|\sum_j U_{ij}U^*_{kj}|$ for $i \neq k$) and distinct columns ($|\sum_i U_{ij}U^*_{ik}|$ for $j \neq k$), which must vanish identically for a unitary matrix. We have computed these using the corresponding values of the matrix and listed them in Table 9.

iii. *Global Frobenius Norms:* The scalar distances $\|UU^\dagger - I_3\|_F$ and $\|U^\dagger U - I_3\|_F$, which integrate all diagonal and off-diagonal departures into a single root-mean-square measure. We have reported these values and placed in Table 10.

Table 8: Diagonal deviations of $UU^\dagger$ (row norms) and $U^\dagger U$ (column norms) from unity.

	Row: $\lvert\sum_j \lvert U_{ij}\rvert^2 - 1\rvert$			Column: $\lvert\sum_i \lvert U_{ij}\rvert^2 - 1\rvert$		
Ordering	Row 1	Row 2	Row 3	Col 1	Col 2	Col 3
NO	1.8×10^{-4}	1.0×10^{-4}	1.2×10^{-4}	1.4×10^{-4}	3.2×10^{-4}	6.0×10^{-5}
IO	1.7×10^{-4}	9.0×10^{-5}	1.3×10^{-4}	1.6×10^{-4}	3.0×10^{-4}	6.0×10^{-5}

Table 9: Off-diagonal deviations of $UU^\dagger$ (row pairs) and $U^\dagger U$ (column pairs) from zero.

	Row pairs $\lvert\sum_j U_{ij}U_{kj}^*\rvert$			Column pairs $\lvert\sum_i U_{ij}U_{ik}^*\rvert$		
Ordering	(e,μ)	(e,τ)	(μ,τ)	$(1,2)$	$(1,3)$	$(2,3)$
NO	8.1×10^{-5}	2.5×10^{-5}	1.8×10^{-4}	2.3×10^{-4}	8.0×10^{-6}	1.1×10^{-5}
IO	5.0×10^{-5}	5.3×10^{-5}	1.8×10^{-4}	2.2×10^{-4}	1.0×10^{-5}	5.0×10^{-6}

Table 10: Frobenius norm of the unitarity deviation for both row and column unitarity conditions.

Ordering	$\lVert UU^\dagger - I_3\rVert_F$	$\lVert U^\dagger U - I_3\rVert_F$
NO	3.1×10^{-4}	4.2×10^{-4}
IO	3.0×10^{-4}	4.1×10^{-4}

As reported in Table 8, all six diagonal deviations lie tightly between 6×10^{-5} and 3.2×10^{-4} for both mass orderings. Similarly, the off-diagonal inner products (Table 9) remain strictly bounded, ranging from 5×10^{-6} to 2.3×10^{-4}. The global Frobenius norms (Table 10) confirm that $\lVert UU^\dagger - I_3\rVert_F \approx 3.0$–$3.1 \times 10^{-4}$ and $\lVert U^\dagger U - I_3\rVert_F \approx 4.1$–$4.2 \times 10^{-4}$, demonstrating that row and column unitarity conditions are satisfied to an equivalent degree.

To rigorously account for these non-zero residuals, we evaluate the propagation of numerical input rounding. Because each input mixing angle is rounded to three significant figures, the maximum uncertainty on any matrix element modulus is $\Delta|U_{ij}| \approx 0.0005$. This propagates to a baseline completeness sum uncertainty of $\sigma\left(\sum_j |U_{ij}|^2\right) \approx 0.001/\sqrt{3} \approx 5.8 \times 10^{-4}$. Every residual observed in Tables 8–10 lies well within this rounding budget.

The three independently derived and calculated mixing angles therefore automatically satisfy probability conservation for both mass orderings without requiring any manual or forced unitarity constraints to be imposed on the derivation. This internal coherence provides strong independent validation for the validity of the analytic formulation.

4.4 Quark–Lepton Duality and $(B - L)$ Gauge Charge

The structural contrast between the CKM and PMNS matrices arises from a difference in their coupling factor:

$$\mathcal{C} = 1 + \frac{B - L}{2}. \tag{73}$$

Table 11 places the two mixing sectors side by side under this equation. This presentation reveals their common geometric origin. The Jarlskog invariant row provides the most striking entry. The

ratio satisfies $|J^{\ell}_{\rm CP}/J^{q}_{\rm CP}| \approx 10^3$. This three-order-of-magnitude difference originates from a sign flip in the $(B-L)$ gauge charge. The lepton sector possesses $D_\ell/2 = -1/2$. This charge sets $\mathcal{C}_\ell = 1/2$ in a compliant vacuum. The quark sector possesses $D_q/2 = +1/6$. This charge sets $\mathcal{C}_q = 7/6$ in a rigid vacuum. Both the CKM and PMNS matrices are expressible in terms of λ, α_q, and α_l alone; the coupling factor $\mathcal{C} = 1 + (B-L)/2$ is the sole differentiator between the sectors. Table 12 provides the key quark–lepton mixing observables expressed using λ, α_q and α_ℓ.

Table 11: Quark–Lepton Duality in the Analytical Framework.

Property	Quark Sector $(B = \frac{1}{3}, L = 0)$	Lepton Sector $(B = 0, L = 1)$
$(B-L)$ gauge charge	$D_q = +1/3$	$D_\ell = -1$
Coupling factor $\mathcal{C}$	$7/6 > 1$ (Rigid)	$1/2 < 1$ (Compliant)
Charge-Neutral Isospin Point	$T_3^{(0)} = -1/6$ ($\theta_0 \approx 109.5°$)	$T_3^{(0)} = +1/2$ ($\theta_0 = 0°$)
Primary Angle	$\sin\theta^q_{12} \approx 0.225$ (Small)	$\sin\theta^\ell_{12} \approx 0.555$ (Large)
2–3 Mixing	$\sin\theta^q_{23} \approx 0.041$ (Hierarchical)	$\sin\theta^\ell_{23} \approx 0.742$ (Upper octant)
Jarlskog Invariant	$J^q_{\rm CP} \approx +3.01 \times 10^{-5}$	$J^\ell_{\rm CP} \approx -0.0321$ (IO); -8.58×10^{-4} (NO)
Equilibrium mixing-weight	$\alpha_q \approx 0.063084$, $\alpha_q(1-\alpha_q) = \frac{7}{6\pi^2}$	$\alpha_l \approx 0.0260$, $\alpha_l(1-\alpha_l) = \frac{1}{4\pi^2}$

Table 12: Mixing observables expressed in terms of the universal invariants λ, α_q.

Observable	Analytical formula	Sector
Cabibbo scale (CKM)	$\lambda = 1/(\pi\sqrt{2})$	Quark
$\lvert V_{cb}\rvert$ (CKM)	$\lambda^2(1-\lambda)(1+\alpha_q)$ / row-norm	Quark
$\lvert V_{ub}\rvert$ (CKM)	$\lambda^3/3$ / row-norm	Quark
$\sin^2\theta_{12}$ (PMNS)	$\frac{1}{3} - \alpha_l(1-\alpha_l) = \frac{1}{3} - \frac{1}{4\pi^2}$	Lepton
$\sin^2\theta_{13}$ (PMNS)	$\alpha_l(1-\alpha_l) - \frac{\lambda^3}{3} = \frac{1}{4\pi^2} - \frac{\lambda^3}{3}$	Lepton
$\sin^2\theta_{23}$ (PMNS)	$\frac{1}{2} + 2\alpha_l(1-\alpha_l) = \frac{1}{2} + \lambda^2$	Lepton
$\delta^{\rm CKM}_{\rm CP}$	$\arcsin(1-\alpha_q) \approx 69.55°$	Quark
$\delta^{\rm PMNS}_{\rm CP,NO}$	$180° + \arcsin(\alpha_l) \approx 181.49°$	Lepton
$\delta^{\rm PMNS}_{\rm CP,IO}$	$360° - \arcsin(1-\alpha_l) \approx 283.10°$	Lepton
$\alpha_q(1-\alpha_q) = \mathcal{C}_q\lambda^2 = \frac{7}{12\pi^2}$ (Quark),	$\alpha_l(1-\alpha_l) = \mathcal{C}_\ell\lambda^2 = \frac{1}{4\pi^2}$ (Lepton)	

5 Conclusions and Outlook

In this work, we have generalized the quark sector *mixing equilibrium condition* of the companion work [21], postulating it as

$$\alpha_i(1-\alpha_i) = \mathcal{C}_i\lambda^2,$$

where $i = q$ and $i = \ell$ for quarks and leptons, respectively, to include both sectors. Here, $0 < \alpha_i < 1-\alpha_i$ represents the *equilibrium mixing-weight*, $(1-\alpha_i)$ is the *equilibrium retention-weight*, and $\mathcal{C}_i = 1 + (B-L)_i/2$ is the *coupling factor* with $(B-L)_i$ denoting the gauge charge of the

respective sector. The same fermion mixing constant $\lambda = 1/(\pi\sqrt{2})$ appears in the generalized mixing equilibrium condition of both sectors.

Using this condition, we establish the closed-form expressions for all three mixing angles and the Dirac CP phase associated with the PMNS lepton mixing matrix using λ and α_ℓ. Since λ is a sector-invariant constant, the mixing behaviour of the quark and lepton sectors is distinguished by the coupling factor $\mathcal{C}_i = 1 + (B - L)/2$ of the respective sector. The sector coupling factors $\mathcal{C}_q = 7/6$ (quarks) and $\mathcal{C}_\ell = 1/2$ (leptons) represent primary sector identity. We find that $\mathcal{C}_q$ is more than twice (nearly 2.3 times) that of $\mathcal{C}_\ell$. This results in a smaller equilibrium weight and a larger retention-weight for leptons. From the mixing equilibrium condition $\alpha_\ell(1 - \alpha_\ell) = \mathcal{C}_\ell\lambda^2 = 1/(4\pi^2)$, we calculate $\alpha_\ell \approx 0.026000$, with its complement $1 - \alpha_\ell \approx 0.974000$, and find that α_ℓ is smaller than the corresponding quark parameter $\alpha_q \approx 0.063084$ by almost a factor of 2.4. This results in relatively larger solar and atmospheric mixing angles compared to those of the quark sector.

The leptonic Dirac CP phases are obtained as $\delta_{\mathrm{CP,NO}} = 180^\circ + \arcsin(\alpha_\ell) \approx 181.49^\circ$ and $\delta_{\mathrm{CP,IO}} = 360^\circ - \arcsin(1 - \alpha_\ell) \approx 360^\circ - 76.9^\circ = 283.1^\circ$. This mapping of the Dirac CP phases for the IO and NO branches to the mixing-weight and retention-weight corresponding to the mixing equilibrium condition is a direct consequence of the equilibrium condition.

Together with the construction of the CKM quark mixing matrix in the companion paper, this work establishes a unified foundation for electroweak flavour physics, where both the CKM and PMNS matrices of the Standard Model are expressed through a single fermion mixing constant λ without any free parameters or empirical flavour data. The disparate mixing patterns of quarks and leptons are distinguished by their sector coupling factors, $\mathcal{C}_q = 7/6$ (rigid for quarks) and $\mathcal{C}_\ell = 1/2$ (compliant for leptons), computed directly from the $(B - L)$ quantum number of each sector.

The formulation is falsifiable and yields four specific predictions testable at forthcoming neutrino facilities. The atmospheric angle $\sin^2\theta_{23} \approx 0.5507$ ($\theta_{23} \approx 47.91^\circ$) lies in the upper octant; DUNE and Hyper-K can resolve the octant ambiguity and distinguish this prediction from NuFIT IO (0.578) and NO (0.563). The Dirac CP phases are testable through the leptonic CP asymmetry in $\nu_\mu \to \nu_e$ versus $\bar{\nu}_\mu \to \bar{\nu}_e$ appearance channels at DUNE and T2K-II, which will discriminate the ordering and pin down the phase to $\pm 5^\circ$–10°. The solar angle $\sin^2\theta_{12} = 1/3 - 1/(4\pi^2) \approx 0.3080$ will be probed to sub-percent precision by JUNO, providing a clean null-test of the tribimaximal-variance prediction.

Declarations

Competing Interests The author has no competing interests and no conflicts of interest to declare that are relevant to the content of this article.

Funding The author did not receive support from any organization for this work. No funding was received to assist with the preparation of this manuscript.

Ethics Approval Not applicable. This study does not involve human participants or animals.

Consent to Participate Not applicable.

Consent for Publication Not applicable. The author is the sole author and is submitting this paper.

Availability of Data and Materials Not applicable. All data generated or analyzed during this study are included in this article.

Code Availability Not applicable. No data analysis is involved. Any code, if required, will be provided by the author.

Authors' Contributions The author is the sole author and the sole contributor of this paper.

References

[1] Z. Maki, M. Nakagawa, and S. Sakata, "Remarks on the Unified Model of Elementary Particles," *Prog. Theor. Phys.* **28**, 870 (1962), doi:10.1143/PTP.28.870.

[2] C. Giganti, S. Lavignac, and M. Zito, "Neutrino oscillations: the rise of the PMNS paradigm," *Prog. Part. Nucl. Phys.* (2017), doi:10.1016/j.ppnp.2017.10.001.

[3] Y. Fukuda *et al.* (Super-Kamiokande Collaboration), "Evidence for Oscillation of Atmospheric Neutrinos," *Phys. Rev. Lett.* **81**, 1562 (1998), doi:10.1103/PhysRevLett.81.1562.

[4] Q. R. Ahmad *et al.* (SNO Collaboration), "Measurement of the Rate of $\nu_e + d \to p + p + e^-$ Interactions Produced by ^{8}B Solar Neutrinos," *Phys. Rev. Lett.* **87**, 071301 (2001), doi:10.1103/PhysRevLett.87.071301.

[5] K. Eguchi *et al.* (KamLAND Collaboration), "First Measurement of Reactor Anti-neutrino Disappearance," *Phys. Rev. Lett.* **90**, 021802 (2003), doi:10.1103/PhysRevLett.90.021802.

[6] F. P. An *et al.* (Daya Bay Collaboration), "Observation of Electron-Antineutrino Disappearance at Daya Bay," *Phys. Rev. Lett.* **108**, 171803 (2012), doi:10.1103/PhysRevLett.108.171803.

[7] B. Pontecorvo, "Mesonium and Anti-mesonium," *Sov. Phys. JETP* **6**, 429 (1957).

[8] S. Navas *et al.* (Particle Data Group), "Review of Particle Physics," *Phys. Rev. D* **110**, 030001 (2024), doi:10.1103/PhysRevD.110.030001.

[9] Z.-Z. Xing, "A new Wolfenstein-like expansion of lepton flavour mixing towards understanding its fine structure," *Phys. Lett. B* (2024), doi:10.1016/j.physletb.2024.138681.

[10] G. Dattoli and K. Zhukovsky, "Neutrino mixing and the exponential form of the Pontecorvo–Maki–Nakagawa–Sakata matrix," *Eur. Phys. J. C* **55**, 547 (2008), doi:10.1140/epjc/s10052-008-0620-8.

[11] Y. Hosotani, "Neutrino oscillations and PMNS matrix in gauge-Higgs unification," *Phys. Rev. D* **113**, 035013 (2026), doi:10.1103/cs4b-n8wf.

[12] G. Altarelli and F. Feruglio, "Discrete Flavour Symmetries and Models of Neutrino Mixing," *Rev. Mod. Phys.* **82**, 2701 (2010), doi:10.1103/RevModPhys.82.2701.

[13] H. Ishimori *et al.*, "Non-Abelian Discrete Symmetries in Particle Physics," *Prog. Theor. Phys. Suppl.* **183**, 1 (2010), doi:10.1143/PTPS.183.1.

[14] S. F. King and C. Luhn, "Neutrino Mass and Mixing with Discrete Symmetries," *Rept. Prog. Phys.* **76**, 056201 (2013), doi:10.1088/0034-4885/76/5/056201.

[15] A. Giarnetti, S. Marciano, and D. Meloni, "On Quark–Lepton Mixing and the Leptonic CP Violation," *Universe* (2024), doi:10.3390/universe10090345.

[16] B. Lampe, "Analytic and Parameter-Free Formula for the Neutrino Mixing Matrix," arXiv:2308.08498 (2023).

[17] R. B. Holmes, "Method for Fitting and Deriving the CKM and PMNS Matrices from Underlying Wavefunctions," *J. Mod. Phys.* (2024), doi:10.4236/jmp.2024.1513099.

[18] F. Potter, "Geometrical Derivation of the Lepton PMNS Matrix Values," *Proc. NPA* **10**, 29 (2013).

[19] M. Raidal, "Relation Between Quark and Lepton Mixing Angles," *Phys. Rev. Lett.* **93**, 161801 (2004), doi:10.1103/PhysRevLett.93.161801.

[20] H. Minakata and A. Y. Smirnov, "Quark–Lepton Complementarity and Self-Complementarity," *Phys. Rev. D* **70**, 073009 (2004), doi:10.1103/PhysRevD.70.073009.

[21] P. K. Meher, "Analytical Construction of the CKM Matrix Using a Single Electroweak Constant," Research Square Preprint, doi:10.21203/rs.3.rs-10958134/v1.

[22] M. Gell-Mann, "The Interpretation of the New Particles as Displaced Charge Multiplets," *Nuovo Cim. Suppl.* **4**, 848 (1956), doi:10.1007/BF02748000.

[23] K. Nishijima, "Charge Independence Theory of V Particles," *Prog. Theor. Phys.* **13**, 285 (1955), doi:10.1143/PTP.13.285.

[24] M. E. Peskin and D. V. Schroeder, *An Introduction to Quantum Field Theory*, Addison-Wesley, Reading, MA (1995).

[25] I. Esteban, M. C. Gonzalez-Garcia, M. Maltoni, I. Martinez-Soler, and T. Schwetz, "NuFIT 6.0: Global Analysis of Three-Flavour Neutrino Oscillations," *JHEP* **12**, 216 (2024), doi:10.1007/JHEP12(2024)216, arXiv:2410.05380 [hep-ph].